Influence of Periodic Cyclic Loading and Rest Period on Soft Clay Consolidation

Shashika Atapattu

PhD Student,

School of Civil and Environmental Engineering, University of Technology Sydney, Ultimo, NSW 2007, Australia

Buddhima Indraratna[1]

Distinguished Professor of Civil Engineering, and Director,

Transport Research Centre, University of Technology Sydney, Ultimo, NSW 2007, Australia

Cholachat Rujikiatkamjorn

Professor,

School of Civil and Environmental Engineering, University of Technology Sydney, Ultimo, NSW 2007, Australia

Words: 4285

Figures: 9

Submitted to: Ground Improvement

[1]Corresponding author: Buddhima Indraratna (e-mail: buddhima.indraratna@uts.edu.au)

Abstract

Railways are often subjected to periodic cyclic loading and intermittent rest periods. Excessive consolidation settlements can affect the performance of railway tracks built on the soft subgrade. The consolidation behavior under railway loading conditions with rest periods has not been evaluated thoroughly. In this study, laboratory testing was conducted to investigate the influence of periodic cyclic loading and rest periods on the consolidation of Holocene soft clay from Ballina NSW. The specimens were subjected to a loading frequency of 1Hz for 54hrs with multiple rest periods. The recorded settlements and excess pore water pressures (EPWP) during cyclic consolidation were employed to determine the corresponding hydraulic gradient, void ratio, resilient (dynamic) modulus and damping ratio. The settlement and accumulated EPWP can be observed during cyclic loading. In contrast, settlements do not occur within a rest period, despite the rapidly dissipating EPWP at the start of a given rest period. The maximum EPWP and settlements decrease as the number of resting periods increases. An analytical model capturing the effect of cyclic loading and rest period is proposed where the unique relationships between the hydraulic gradient and the flow rate are established.

Keywords: Clays, Consolidation, Railway tracks

Notation

AOS	apparent opening size
c_c	coefficient of compressibility
c_{cyc}	coefficient of consolidation under cyclic loading
CL	stage number of cyclic loading

c_v	coefficient of consolidation
dQ	change of volume
DR	damping ratio
DR_1	damping ratio of frist cycle
e	void ratio
E_d	axial dynamic modulus
$E_{d,1}$	axial dynamic modulus of first cycle
EPWP	excess pore water pressure
H	sample height/thickness
H_D	drainage length
k	permeability of the soil
LL	liquid limit
m_{cyc}	coefficient of volume compressibility
PL	plastic limit
q	flow rate
RP	stage number of rest period
$s_{t_{cyc}}$	accumulated settlement at time t
t	time
t_i	time elapsed at an individual period of cyclic load

T_v	time factor
U	degree of consolidation
u	pore pressure
u_A	accumulation of excess pore pressure
u_D	dissipation of excess pore pressure
u_G	generation of excess pore pressure
u_{max}	maximum pore pressure
u_r	residual excess pore water pressure
W	stored energy
α	experimental constant
β	experimental constant
γ_w	unit weight of water
Δe	change in void ratio
Δu	change of excess pore water pressure
$\Delta\sigma'_{cyc}$	increase in effective stress due to cyclic loading
$\varepsilon_{z,initial}$	initial axial strain in each cycle
$\varepsilon_{z,max}$	maximum axial strain in each cycle
$\varepsilon_{t_{cyc}}$	vertical strain at time t
η	experimental constant

λ	relative void ratio
σ'_0	initial effective stress
σ_0	applied preconsolidation stress
$\sigma_{v,cyc}$	cyclic vertical stress
$\sigma_{z,initial}$	initial axial stress in each cycle
$\sigma_{z,max}$	maximum axial stress in each cycle

1. Introduction

Settlement of railway tracks built on soft soils can lead to instability, high maintenance costs, and service disruption. In the eastern coastal regions of Australia, relatively thick, soft Holocene clay layers (up to 30m deep) can be found with intermittent sand layers (Indraratna et al., 2013; Kelly et al., 2017; Lim et al., 2018; Pineda et al., 2016). Typically, these clay layers have relatively low permeability and high compressibility. When such clays are subjected to cyclic train loading under poor drainage conditions, excess pore water pressures (EPWP) accumulate with time, causing instability such as differential settlement, undrained failure and subgrade fluidisation (Ansal & Erken, 1989; Brown et al., 1975; Diaz-Rodriguez, 1989; Duong et al., 2014; Indraratna, Singh, et al., 2020).

In railway embankments built on soft clay deposits, consolidation deformation can be significant. The behaviour of clayey soils subjected to static embankment loads is usually well-understood, and various design techniques reported in past literature are presented, and they explain how the post-construction consolidation settlement can be controlled (Arulrajah et al., 2009; Indraratna et al., 2005; Kelly et al., 2018; Mesri & Choi, 1985; Ngo et al., 2020). Besides, the assessment of settlement behaviour under cyclic loading becomes a challenging task due to (i) time-dependent EPWP accumulation behaviour (Indraratna et al. 2020; Duong et al. 2014; Ni 2012); (ii) Stiffness variation (Andersen, 2015; Cai et al., 2018). With the increasing number of loading cycles, soil behaviour continues to vary depending on the magnitude and frequency of the applied load. Therefore, the consolidation settlement of railway tracks would be required to be assessed under a more realistic cyclic loading rather than static loading.

In view of the above, the scope of this study is to investigate the consolidation behaviour under railway loading conditions. Although a considerable amount of research has been carried out to investigate the undrained behaviour (i.e. no volume reduction) of soft soils under cyclic loading, their consolidation under railway loading conditions with special reference to rest periods has not been evaluated thoroughly. This study aims to provide further insight into consolidation settlement and corresponding EPWP under periodic cyclic loading capturing the influence of rest periods.

A summary of consolidation tests performed under cyclic/repeated loading conditions is provided in Table 1. Brown et al. (1977) investigated the consolidation behavior under long-term repeated loading conditions using cyclic triaxial testing with a loading frequency of 0.1 Hz, and their results showed that drainage during the rest period (i.e., no loading) would increase the stiffness of clay when subjected to subsequent cyclic loading. Geng et al. (2006), Yıldırım & Erşan (2007), Toufigh & Ouria (2009), Chai et al. (2021) studied consolidation under low-frequency loading (≤ 0.1 Hz) and proposed theoretical solutions for cyclic consolidation. Through a series of undrained cyclic triaxial testing, Zhou & Gong (2001) and Indraratna et al. (2020) showed that loading amplitude and frequency had a significant effect on the development of axial strains. Furthermore, Yasuhara et al. (1982) and Ni (2012) confirmed that higher frequencies may delay the development of the peak EPWP under undrained conditions. Lei et al. (2020) investigated the cyclic behavior of soft clay under intermittent cyclic loading; here the frequencies were varied from 0.5 to 2 Hz under undrained conditions with intermittent rest periods, however, drainage was allowed while a static load equivalent to half of the cyclic loading was maintained. A similar loading condition was also adopted by Liu & Xue (2022), Li et al. (2021) and Nie et al. (2020), where drainage period between loading cycles can improve the cyclic resistance of clay for subsequent loading cycles. However, the above studies do not represent the actual railway loading conditions. Loading frequency in railway subgrade varies between 1 – 5 Hz when a train travelling approximately at 45-225 km/h (Arivalagan et al., 2021; Indraratna et al., 2020; Mamou et al., 2017; Powrie et al., 2007).

2. Theoretical development

Model description

Cyclic loading with drainage can cause consolidation settlement via EPWP dissipation. EPWP dissipation during rest periods without any live loading causes negligible deformation, so the observed behaviour in the subsequent section can be conceptualised as illustrated in Figure 1 using the piston analogy. At the initial stage (Figure 1(a)), the effective stress (σ'_0) of the normally consolidated soil is equal to the applied preconsolidation stress (σ_0) with no EPWP (Δu = 0). When the cyclic load is applied, say due to the passage of a train (Figure 1(b)), soil settlement occurs while the EPWP starts to accumulate during the loading-unloading process, as the rate of pore pressure generation rate is higher than its rate of dissipation. Simultaneously, settlement causes a reduction in void ratio, contributing to an increase in effective stress ($\sigma'_{t1} = \sigma'_{t0} + \Delta\sigma'_{cyc}$); where $\Delta\sigma'_{cyc}$ is the increase in effective stress due to cyclic loading as a function of the change of void ratio, (Δe). When the cyclic loading ceases during the rest period (Figure 1(c)), the accumulated EPWP (Δu_t) starts to decrease to reach an equilibrium (i.e., $\Delta u_t \rightarrow u_r$) as shown in Figure 1(d). The removal of cyclic load contributes to swelling (i.e., $\Delta e \rightarrow \Delta e^*$), the extent of which depends on the type of soft soil and the magnitude of stress release; however, in this study, swelling (within 0.05 mm) is considered negligible based on the experimental results as presented in the following section of the paper.

Determination of time-dependent settlement due to EPWP dissipation during cyclic load

The processes of EPWP generation and dissipation as well as volumetric strain under cyclic load, are presented in Fig. 2 (Hyodo & Yasuhara, 1988). In this study, we consider that the settlement only occurs due to the dissipation of EPWP. For a given cyclic vertical stress ($\sigma_{v,cyc}$), the coefficient of volume compressibility for one-dimensional compression under the small strain condition can be determined by:

$$m_{cyc} = \frac{\varepsilon_f}{\sigma_{v,cyc}} \tag{1}$$

where ε_f is the final vertical strain due to the cyclic vertical stress.

The strain-based degree of consolidation (U) at a vertical strain ($\varepsilon_{t_{cyc}}$) upon an accumulated time during cyclic loading (t_{cyc}) can be obtained from:

$$U = \frac{\varepsilon_{t_{cyc}}}{\varepsilon_f} = \frac{s_{t_{cyc}}}{m_{cyc}\sigma_{v,cyc}H} \tag{2}$$

where $s_{t_{cyc}}$ and H are the accumulated settlement during cyclic load and the sample height, respectively.

It is assumed that the degree of consolidation based on Terzaghi's 1-D consolidation theory (Terzaghi, 1943) can be expressed by:

$$U = 1 - \sum_{m=0}^{\infty} \frac{2}{M^2} \exp(-M^2 T_v) \quad (3a)$$

$$T_v = \frac{c_{cyc} t_{cyc}}{H_{dr}^2} \quad (3b)$$

where, T_v is the time factor and c_{cyc} is the coefficient of consolidation which can be back-analysed using time-settlement curve and Eqs. (1)-(3).

Determination of time-dependent EPWP due to cyclic load

Based on Fig. 2, the accumulation of excess pore pressure (u_A) can be calculated based on the difference between the generation (u_G)and dissipation (u_D) of EPWP as:

$$u_A = u_G - u_D \quad (4)$$

The dissipation of EPWP can be obtained using time-dependent settlement by:

$$u_D = \frac{\varepsilon_{t_{cyc}}}{\varepsilon_f} \sigma_{v,cyc} \quad (5)$$

Based on Laboratory observation, u_A follows an exponential relationship with time elapsed at an individual period of cyclic load (t_i) and can be expressed as:

$$\frac{u_A}{u_A^{max}} = 1 - \alpha e^{-\beta t_i} \quad (6)$$

where u_A^{max} is the measured maximum accumulation of EPWP at an individual period of cyclic load and α, β are experimental constants. Subsequent experimental results show that u_A^{max} is a function of the void ratio during cyclic loading.

A theoretical model for EPWP dissipation during the rest period

During the rest period, no volumetric strains of the soil occur as described in Figure 1. Therefore, pore fluid is considered slightly compressible and the volume change in the pore fluid is considered equal to the flow rate during a given time interval (*dt)*. If the change of volume and flow rate per unit volume are *dQ* and *q*, respectively, the continuity equation of the soil specimen with thickness dz can be represented by;

$$dQ = \frac{\partial q}{\partial z} dzdt \tag{7}$$

Considering Darcy's law;

$$q = \frac{k}{\gamma_w} \frac{\partial u}{\partial z} \tag{8}$$

where γ_w is the unit weight of water, u is the EPWP and *k* is the permeability of the soil. Eqs. (7) and (8) can be combined and re-written as;

$$dQ = \frac{k}{\gamma_w} \frac{\partial^2 u}{\partial z^2} \tag{9}$$

The change in EPWP can result in a change in the volume of pore fluid per unit volume, therefore;

$$dV = \frac{\mu_s}{\gamma_w} \frac{\partial u}{\partial t} dzdt \tag{10}$$

where *u* is the pore pressure at time *t* and depth *z*. By combining Equations (9) and (10), the Equation for the one-dimensional EPWP transmission during the rest period can be obtained as:

$$\frac{\partial u}{\partial t} = \eta \frac{\partial^2 u}{\partial z^2} \quad ; \eta = \frac{k}{\mu_s} \tag{11}$$

Constant η determines the rate of the pore pressure dissipation. It should be noted that, Equation (11) has the same form as Terzaghi's one-dimensional consolidation equation. However, this Equation considers that the pore fluid deformation is elastic and the pore volume change occurs due to the elastic deformation of the fluid as a result of stress removal in the rest period. It is important to note that, this volume change is tiny as the compressibility of the water is significantly high. Further, the volume of the solid is considered to be unchanged.

To solve Eq (11), a soil element under two-way drainage is considered. Assuming that the pore pressure behaviour is symmetrical along the mid-depth, thickness, H is considered where H_D = Half of the full thickness of the soil section. The following initial conditions and boundary conditions are established.

$$\begin{cases} u = 0\ (t = 0, z = 0) \\ u = f(z)\ (t = 0, 0 < z \leq H_D) \end{cases} \tag{12}$$

$$\begin{cases} u = 0\ (0 < t \leq \infty, z = 0) \\ \frac{\partial u}{\partial z} = 0\ (0 < t \leq \infty, z = H_D) \end{cases} \tag{13}$$

where $f(z)$ is the non-uniform distribution of the excess pore pressure with depth due to the cyclic load application. Assuming the excess pore pressure distribution is sinusoidal, and excess pore pressure is zero at the drainage boundary;

$$f(z) = u_1 sin\left(\frac{\pi z}{2H_D}\right) \tag{14}$$

where u_1 is the measured excess pore pressure at depth H_D, at $t = 0$.

2. Experimental program

To overcome the limitations of conventional oedometers and Rowe cells for which cyclic loading cannot be applied, the Dynamic Filtration Apparatus (DFA) developed by Israr et al. (2016) and later used extensively by Arivalagan et al. (2021, 2022) was modified to investigate one-dimensional cyclic consolidation behavior. This unique apparatus (Figure 3) consisted of 4 main components; (1) hydraulic actuator, (2) piston, (3) rigid loading plate, and (4) polycarbonate rigid cell. The polycarbonate cell had an internal diameter of 240 mm, a height of 300 mm, and a thickness of 13 mm. In the current study, a linear variable differential transformer (LVDT) was attached to the axial hydraulic actuator to measure the settlement of the soil specimen. Two body pressure transducers attached to the periphery of the polycarbonate cell (1 kPa accuracy) were used to measure the excess pore water pressure. Pore pressure transducers (P1 and P2) were located near the top-sand-clay interface and at 35 mm above the bottom sand-clay interface, respectively. A volumetric flask was connected to the bottom drainage to collect the discharge. Cyclic vertical load was applied using the hydraulic actuator via the rigid loading plate through the piston. A compacted coarse sand layer was used as the drainage layer at the top and the bottom of the clay specimen (i.e., two-way drainage).

Reconstituted clay samples at Ballina NSW (1.3 m to 2.2 m deep) were used during testing. The soil specimen was characterized by a clay fraction of 25%, with a liquid limit, plastic limit and natural water content of 82%, 29%, and 70%, respectively. According to the Unified Soil Classification System (USCS), this soil could be classified as high-plasticity clay (CH). The test samples were mixed with de-aired distilled water at 1.2 times the liquid limit to form a slurry, which was kept for 24 hours in air-tight containers stored in a humidity-controlled room. The initial void ratio of the slurry was 2.61, and under a consolidation pressure of 50 kPa following ASTM-D2435 (ASTM-D2435, 2010) coefficient of compressibility (c_c) of 0.47 and coefficient of consolidation (c_v) of 1.19 m^2/year could be determined.

The test procedure is briefly described as follows:

1. The internal wall of the polycarbonate cell was coated with Teflon to minimise boundary friction between the cell wall and test specimen. Then, a coarse sand layer

was compacted in three layers at the cell’s bottom to a thickness of 40 mm, and saturated with distilled water. Sand layers were compacted using the 2.5-kg top loading plate with a detachable handle to lift the loading plate. Drop height (300 mm) and the number of drops (50) were selected to achieve the standard compaction energy of 600 kN-m/m^3 (ASTM-D698, 2012). A permeable geotextile was placed on top of the sand layer to prevent any intermixing between clay and sand layers (apparent opening size, AOS of the geotextile was <1 µm; minimum particle size of clay = 1 µm and that of sand = 0.2 mm).

2. The clay slurry was poured into the cell until a total specimen height of 135 mm was attained. A permeable geotextile layer was then placed on top of the clay slurry, and the top sand layer was carefully compacted to a thickness of 20 mm. The specimen was consolidated by applying a pressure of 25 kPa representing an in-situ pressure corresponding to a depth of 1.5 m. Preconsolidation was continued until a negligible rate of settlement (i.e. <0.1 mm/h) and complete dissipation of EPWP (< 1 kPa) was achieved, thus giving a final specimen height of 90 mm with an initial void ratio of 1.41 evaluated from weight-volume relationships.

3. In addition to the initial vertical stress of 25 kPa, a vertical sinusoidal cyclic load (amplitude = 40 kPa, frequency = 1 Hz) was applied, resulting in minimum and maximum vertical stresses of 25 and 65 kPa, respectively. These loading conditions conformed to 25-tonne axle loading of a heavy haul train travelling at 45 km/h (Indraratna et al. 2020; Powrie et al. 2007).

To simulate typical heavy haul operations on a track built on soft subgrade, the cyclic loading was applied during normal operating hours of the laboratory and a rest period was maintained overnight, as shown in Figure 4(a) for 5 sets of this cyclic loading pattern. CL and RP represent the stage number of cyclic loading and rest period, respectively.

3. Experimental results

3.1 EPWP, settlements, and void ratio

As shown in Figure 4(b), the measured EPWP is the difference between the built-up and dissipated ones. As expected, EPWP near the drainage (P1) rises quickly and dissipates during the application of cyclic loading. In contrast, EPWP gradually increases despite the proximity to drainage boundary (35 mm away from P2). During CL3, CL4 and CL5, the drop in the EPWP can be observed after 30,000 cycles. This indicates that the magnitude of EPWP dissipation is greater than the EPWP generation (Figure 4(b)) and results in an overall reduction of the EPWP. The decrease in void ratio through settlement during the previous cyclic loading and the dissipation of EPWP during rest period causes lesser accumulated EPWP in the following loading stage. This can also be attributed to the inevitable increase in soil stiffness (reduction in pore space/void ratio) during cyclic consolidation. As expected, at the drainage boundary, the EPWP is minimal (0.6 - 1.6 kPa).

In Figure 4(c), settlements are observed to be substantial in CL1 and they gradually reduce during the subsequent loading stages. This can also be confirmed by the reduction in the measured discharge volume from the bottom drainage (Figure 4(d)) as cyclic consolidation occurs to make the soil stiffer. It can be seen that settlement only occurs during the loading application, while there is insignificant deformation during a rest period, and this observation was also reported by Li et al. (2021). A similar behaviour could be observed at a railway site in the town of Sandgate, NSW, where the measured EPWP increased during the passage of a train and then diminished swiftly to the normal hydrostatic level during the rest periods, while the rate of settlement significantly reduced with time (Indraratna et al., 2010).

Furthermore, experimental results show that, normalised EPWP with the maximum EPWP ($1 - u/u_A$), follows an exponential relationship with time elapsed at an individual period of cyclic load (t_i) (Figure 5). This confirms that the rate of EPWP accumulation is relatively constant in all subsequent loading stages.

3.2 Soil behaviour during the rest period

Figure 6(a) shows the measured EPWP at P2 during rest periods. In the absence of loading, redistribution of the EPWP can be observed during the rest periods without any deformation occurring. For instance, the excess pore pressure becomes less than 1 kPa within 13 hours without deformation. This is in contrast to static consolidation, where the dissipation of EPWP generated by sustained external loading can cause notable deformation. Figure 6(b) shows the measured normalised EPWP (the ratio of the EPWP and the initial EPWP of the corresponding loading stage), confirming that the redistribution of EPWP is independent of the initial pore pressure.

The measured EPWP at H_D = 45 mm was adopted to calibrate the proposed model described earlier (Eqs. 11-14). Based on the back analysis, the constant η = 1.42 m^2/year can be obtained. Figure 6(a) compares the predicted model results with the recorded EPWP at the start of rest periods (RP1, RP2, RP3 and RP4), where $u_{1(RP1)}$, $u_{1(RP2)}$, $u_{1(RP3)}$ and $u_{1(RP4)}$, are 22.4 kPa, 16.4 kPa, 11.7 kPa and 7.6 kPa, respectively. An acceptable agreement is established, whereby the proposed EPWP prediction model (including both cyclic loading and rest period) is validated using the experimental data as shown earlier in Figures 4(b) and 4(c). Here the value of m_{cyc} was calculated from Eq. (1) to be 2.58×10^{-3} m^2/kN and the back-calculated value of c_{cyc} was 0.75 m^2/year. The generation of EPWP during cyclic loading was calculated using Eqs. (4-6) where back-calculated α and β parameters are 0.85 and 0.0002, respectively.

3.3 Soil stiffness during cyclic consolidation

To quantify the soil stiffness variation during cyclic loading, the axial dynamic modulus (E_d) was determined using the method proposed by Cai et al. (2018), where E_d = $(\sigma_{z,max} - \sigma_{d,initial})/(\varepsilon_{z,max} - \varepsilon_{z,initial})$; $\sigma_{z,max}$ and $\varepsilon_{z,max}$ = maximum axial stress and strain in each cycle, respectively; $\sigma_{z,initial}$ and $\varepsilon_{z,initial}$ = initial axial stress and strain in each cycle, respectively. Figures 7(a) and 7(b) show the development of the E_d and the normalised modulus ($E_d/E_{d,1}$) with the number of cycles where $E_{d,1}$ is the corresponding value of the 1st cycle. Figure 7(a) shows that, during CL1, the axial dynamic modulus gradually increases with the number of cycles due to the consolidation. The initial $E_d/E_{d,1}$ reduces in the subsequent loading stages as the consolidation progresses.

The damping ratio (DR) was calculated using the ratio between the consumed energy (ΔW) to the stored energy (W) do a given cycle, where DR = $\Delta W/4\pi W$. In contrast to E_d, DR and relative change of damping ratio (DR/DR_1) reduce with the number of cycles and after each rest period (DR_1 is the corresponding value of the 1st cycle). This behaviour is opposite to the measured axial dynamic modulus and damping ratio during undrained cyclic loading, where the axial dynamic modulus decreases with the number of cycles while the damping ratio increases with the number of cycles (Cai et al., 2018; Indraratna et al., 2022; Lei et al., 2020; Nguyen et al., 2021).

The increase in axial dynamic modulus between subsequent loading (ΔE_d) and maximum EPWP (u_{max}) is related to the soil structure, including void ratio. Therefore, the parameter representing the relative void ratio (λ) is introduced to obtain the desired correlation, where

$\lambda = (e_0 - e)/(e_0 - e_f)$; e_0 = initial void ratio; e_f = final void ratio. λ = 0 represents the initial condition of the soil, and λ = 1 represents the final condition. Figures 8(a) and 8(b) show that u_{max} and ΔE_d decrease when λ approaches 1, implying that when soil approaches its maximum contraction (or ultimate consolidation settlement), either negligible or minimal change to the EPWP and stiffness occurs. Figures 8(c) and 8(d) show that, u_{max} is directly proportional to the stiffness increase in the previous loading stages. A similar analogy between the change in void ratio and modulus was also discussed by Park & Santamarina (2019) for sandy soils under one-dimensional compression.

3.4 Hydraulic gradient and flow rate during cyclic consolidation

The hydraulic gradient was calculated using the difference between the measured EPWP at P1 and P2. The flow rate was obtained by converting the rate of settlement (per 100 cycles). Figure 9(a) shows that the hydraulic gradient increases with the number of cycles. During the initial number of loading cycles, EPWP accumulates when the generated EPWP (du_G) exceeds the dissipated EPWP (du_D). In contrast to the consolidation occurring under incremental loading, where the hydraulic gradient is proportional to the flow rate (Hansbo, 1960; Kianfar et al., 2013), the relationship between the hydraulic gradient and the flow rate is inversely proportional as indicated in Figure 9(b). However, when the dissipation rate dominates (i.e. $du_D > du_G$), the hydraulic gradient becomes proportional to the flow rate, which is similar to the condition of static consolidation.

5. Conclusions

This study was focused on the influence of periodic cyclic loading and rest periods on soft soil consolidation in which changes to the excess pore water pressure (EPWP), settlements, void ratio, axial dynamic modulus, and hydraulic gradient were quantified together with their inter-relationships where warranted. The salient findings based on this study are as follows:

1. The development of EPWP, settlements, and vertical strains reduced considerably from cyclic loading-stage 1 to 5 (CL1 to CL5). The maximum EPWP (u_{max}) decreases upon the subsequent loading stages, where u_{max} during CL1 and CL5 were 21.3 kPa and 5.2 kPa, respectively. Similar trends were observed for settlement and discharged water. When the test specimen was subjected to cyclic loading with effective drainage, it became increasingly stiffer due to the consolidation and offered more resistance to the subsequent cyclic load with the corresponding EPWP becoming less than the previous loading stage.

2. Observed settlements and volume outflow from the bottom drain suggest that cyclic consolidation does not occur during the rest periods (i.e., negligible settlement) albeit notable rate of dissipation of the accumulated EPWP. Furthermore, the rate of pore pressure dissipation during rest period was found to be independent of the accumulated EPWP value at the start of the rest period.

3. The axial dynamic modulus increased from 89.9 kPa to 121.7 kPa (approx. 35% increase) and the damping ratio reduced to <10% from its initial value from CL1-CL5. Their relationships with the relative void ratio (λ) could be established where changes were minimum when λ approached 1. This implies that for a given cyclic loading pattern with appropriate rest periods, the extent of change to the dynamic modulus, damping ratio, and EPWP decreases as soil stiffness increases with the number of loading cycles.

4. The hydraulic gradient decreased when the flow velocity increased during the initial phase, when the accumulated EPWP was dominant. However, when the dissipation of EPWP became dominant as facilitated by the drainage, the hydraulic gradient was proportional to the flow velocity as in static loading conditions.

Data Availability

The data used in the current study are available from the corresponding author upon reasonable request.

Acknowledgements

This research was supported by the Australian Government through the Australian Research Council's Linkage and Discovery Projects funding scheme (DP230101769, LP160101254) and the ARC Industrial Transformation Training Centre for Advanced Technologies in Rail Track Infrastructure (ITTC-Rail).

References

Andersen, K. H. (2015). Cyclic soil parameters for offshore foundation design. In *Frontiers in Offshore Geotechnics III - Proceedings of the 3rd International Symposium on Frontiers in Offshore Geotechnics, ISFOG 2015*.

Ansal, A., & Erken, A. (1989). Undrained behavior of clay under cyclic shear stresses. *Journal of Geotechnical Engineering*, *115*(7), 968–983.

Arivalagan, J., Indraratna, B., Rujikiatkamjorn, C., & Warwick, A. (2022). Effectiveness of a Geocomposite-PVD system in preventing subgrade instability and fluidisation under cyclic loading. *Geotextiles and Geomembranes*, *50*(4), 607–617. https://doi.org/10.1016/j.geotexmem.2022.03.001

Arivalagan, J., Rujikiatkamjorn, C., Indraratna, B., & Warwick, A. (2021). The role of geosynthetics in reducing the fluidisation potential of soft subgrade under cyclic loading. *Geotextiles and Geomembranes*, *February*. https://doi.org/10.1016/j.geotexmem.2021.05.004

Arulrajah, A., Abdullah, A., Bo, M. W., & Bouazza, A. (2009). Ground improvement techniques for railway embankments. *Proceedings of the Institution of Civil Engineers: Ground Improvement*, *162*(1), 3–14. https://doi.org/10.1680/grim.2009.162.1.3

ASTM-D2435. (2010). *Standard Test Methods for One-Dimensional Consolidation Properties of Soils Using Incremental Loading*. https://doi.org/10.1520/D2435

ASTM-D698. (2012). *Standard Test Methods for Laboratory Compaction Characteristics of Soil Using Standard Effort (12 400 ft-lbf/ft3 (600 kN-m/m3))*. https://doi.org/10.1520/D0698-12E02

Brown, S. F., Andersen, K. H., & McElvaney, J. (1977). The Effect of Drainage on Cyclic Loading of Clay. *Proceedings of 9th International Conference on Soil Mechanics and Foundation Engineering (Tokyo)*, *118*, 1–6. https://www.issmge.org/publications/online-library

Brown, S. F., Lashine, A. K. F., & Hyde, A. F. L. (1975). Repeated Load Triaxial Testing of a Silty Clay. *Geotechnique*, *25*(1), 95–114. https://doi.org/10.1680/geot.1975.25.1.95

Cai, Y., Wu, T., Guo, L., & Wang, J. (2018). Stiffness Degradation and Plastic Strain Accumulation of Clay under Cyclic Load with Principal Stress Rotation and Deviatoric

Stress Variation. *Journal of Geotechnical and Geoenvironmental Engineering*, *144*(5), 04018021. https://doi.org/10.1061/(asce)gt.1943-5606.0001854

Chai, J. chun, Fu, H. tao, Wang, J., Shen, S. L., & Ding, W. (2021). Method for calculating cyclic load induced 1D and PVD unit cell consolidation deformations. *Computers and Geotechnics*, *136*(January), 104243. https://doi.org/10.1016/j.compgeo.2021.104243

Diaz-Rodriguez, J. A. (1989). Behavior of Mexico City clay subjected to undrained repeated loading. *Canadian Geotechnical Journal*, *26*(1), 159–162. https://doi.org/10.1139/t89-016

Duong, T. V., Cui, Y. J., Tang, A. M., Dupla, J. C., Canou, J., Calon, N., & Robinet, A. (2014). Investigating the mud pumping and interlayer creation phenomena in railway sub-structure. *Engineering Geology*, *171*, 45–58. https://doi.org/10.1016/j.enggeo.2013.12.016

Fujiwara, H., Yamanouchi, T., Yasuhara, K., & Ue, S. (1985). Consolidation of alluvial clay under repeated loading. *Soils and Foundations*, *25*(3), 19–30.

Geng, X., Xu, C., & Cai, Y. (2006). Non-linear consolidation analysis of soil with variable compressibility and permeability under cyclic loadings. *International Journal for Numerical and Analytical Methods in Geomechanics*, *30*(8), 803–821. https://doi.org/10.1002/nag.505

Hansbo, S. (1960). Consolidation of clay with special reference to influence of vertical sand drains. *Swedish Geotechnical Institute Proceeding*, *18*, 45–50.

Hyodo, M., & Yasuhara, K. (1988). Analytical procedure for evaluating pore-water pressure and deformation of saturated clay ground subjected to traffic loads. In *Numerical*

Methods in Geomechanics Innsbruck 1988 (pp. 653–658). Routledge.

Indraratna, B., Korkitsuntornsan, W., & Nguyen, T. T. (2020). Influence of Kaolin content on the cyclic loading response of railway subgrade. *Transportation Geotechnics*, *22*(August 2019), 100319. https://doi.org/10.1016/j.trgeo.2020.100319

Indraratna, B., Qi, Y., Malisetty, R. S., Navaratnarajah, S. K., Mehmood, F., & Tawk, M. (2022). Recycled materials in railroad substructure: an energy perspective. *Railway Engineering Science*. https://doi.org/10.1007/s40534-021-00267-6

Indraratna, B., Rujikiatkamjorn, C., Ewers, B., & Adams, M. (2010). Class A Prediction of the Behavior of Soft Estuarine Soil Foundation Stabilized by Short Vertical Drains beneath a Rail Track . *Journal of Geotechnical and Geoenvironmental Engineering*, *136*(5), 686–696. https://doi.org/10.1061/(asce)gt.1943-5606.0000270

Indraratna, B., Rujikiatkamjorn, C., Geng, X., & Ameratunga, J. (2013). Performance and prediction of vacuum consolidation behavior at Port of Brisbane. *18th International Conference on Soil Mechanics and Geotechnical Engineering: Challenges and Innovations in Geotechnics, ICSMGE 2013*, *3*, 2497–2500. https://ro.uow.edu.au/engpapershttps://ro.uow.edu.au/engpapers/1062https://ro.uow.edu.au/engpapers/1062

Indraratna, B., Rujikiatkamjorn, C., & Sathananthan, L. (2005). Radial consolidation of clay using compressibility indices and varying horizontal permeability. *Canadian Geotechnical Journal*, *42*(5), 1330–1341. https://doi.org/10.1139/t05-052

Indraratna, B., Singh, M., Nguyen, T. T., Leroueil, S., Abeywickrama, A., Kelly, R., & Neville, T. (2020). Laboratory study on subgrade fluidization under undrained cyclic triaxial loading. *Canadian Geotechnical Journal*, *57*(11), 1767–1779. https://doi.org/10.1139/cgj-2019-0350

Israr, J., Indraratna, B., & Rujikiatkamjorn, C. (2016). Laboratory investigation of the seepage induced response of granular soils under static and cyclic loading. *Geotechnical Testing Journal*, *39*(5), 795–812.

Kelly, R. B., Pineda, J. A., Bates, L., Suwal, L. P., & Fitzallen, A. (2017). Site characterisation for the ballina field testing facility. *Geotechnique*, *67*(4), 279–300. https://doi.org/10.1680/JGEOT.15.P.211/ASSET/IMAGES/SMALL/JGEOT.15.P.211-F22.GIF

Kelly, R. B., Sloan, S. W., Pineda, J. A., Kouretzis, G., & Huang, J. (2018). Outcomes of the Newcastle symposium for the prediction of embankment behaviour on soft soil. *Computers and Geotechnics*, *93*, 9–41. https://doi.org/10.1016/j.compgeo.2017.08.005

Kianfar, K., Indraratna, B., & Rujikiatkamjorn, C. (2013). Radial consolidation model incorporating the effects of vacuum preloading and non-Darcian flow. *Geotechnique*, *12*, 1160–1073. https://doi.org/10.1201/b17435-203

Lei, H., Liu, M., Feng, S., Liu, J., & Jiang, M. (2020). Cyclic Behavior of Tianjin Soft Clay under Intermittent Combined-Frequency Cyclic Loading. *International Journal of Geomechanics*, *20*(10), 1–10. https://doi.org/10.1061/(asce)gm.1943-5622.0001805

Li, Y., Nie, R., Yue, Z., Leng, W., & Guo, Y. (2021). Dynamic behaviors of fine-grained subgrade soil under single-stage and multi-stage intermittent cyclic loading: Permanent deformation and its prediction model. *Soil Dynamics and Earthquake Engineering*, *142*(December 2020), 106548. https://doi.org/10.1016/j.soildyn.2020.106548

Lim, G. T., Pineda, J. A., Boukpeti, N., & Carraro, J. A. H. (2018). Predicted and measured behaviour of an embankment on PVD-improved Ballina clay. *Computers and Geotechnics*, *93*, 204–221. https://doi.org/10.1016/j.compgeo.2017.05.024

Liu, Z., & Xue, J. (2022). The deformation characteristics of a kaolin clay under intermittent cyclic loadings. *Soil Dynamics and Earthquake Engineering*, *153*(February 2021), 107112. https://doi.org/10.1016/j.soildyn.2021.107112

Mamou, A., Powrie, W., Priest, J. A., & Clayton, C. (2017). The effects of drainage on the behaviour of railway track foundation materials during cyclic loading. *Geotechnique*, *67*(10), 845–854. https://doi.org/10.1680/jgeot.15.P.278

Mesri, G., & Choi, Y. K. (1985). Settlement analysis of embankments on soft clays. *Journal of Geotechnical Engineering*, *111*(4), 441–464. https://doi.org/10.1061/(ASCE)0733-9410(1985)111:4(441)

Ngo, D. H., Horpibulsuk, S., Suddeepong, A., Hoy, M., Udomchai, A., Doncommul, P., Rachan, R., & Arulrajah, A. (2020). Consolidation behavior of dredged ultra-soft soil improved with prefabricated vertical drain at the Mae Moh mine, Thailand. *Geotextiles and Geomembranes*, *48*(4), 561–571. https://doi.org/10.1016/j.geotexmem.2020.03.002

Nguyen, T. T., Indraratna, B., & Singh, M. (2021). Dynamic parameters of subgrade soils prone to mud pumping considering the influence of kaolin content and the cyclic stress ratio. *Transportation Geotechnics*, *29*(May), 100581. https://doi.org/10.1016/j.trgeo.2021.100581

Ni, J. (2012). Application of geosynthetic vertical drains under cyclic loads in stabilizing tracks. *Doctor of Philosophy Thesis, School of Civil, Mining and Environmental*

Engineering, University of Wollongong, 1–210.

Ni, J., & Geng, X. Y. (2022). Radial consolidation of prefabricated vertical drain-reinforced soft clays under cyclic loading. *Transportation Geotechnics*, *37*(January), 100840. https://doi.org/10.1016/j.trgeo.2022.100840

Nie, R., Mei, H., Leng, W., Ruan, B., Li, Y., & Chen, X. (2020). Characterization of permanent deformation of fine-grained subgrade soil under intermittent loading. *Soil Dynamics and Earthquake Engineering*, *139*. https://doi.org/10.1016/J.SOILDYN.2020.106395

O'reilly, M. P., Brown, S. F., & Overy, R. F. (1991). Cyclic loading of silty clay with drainage periods. *Journal of Geotechnical Engineering*, *117*(2), 354–362. https://doi.org/10.1061/(ASCE)0733-9410(1991)117:2(354)

Park, J., & Santamarina, J. C. (2019). Sand response to a large number of loading cycles under zero-lateral-strain conditions: Evolution of void ratio and small-strain stiffness. *Geotechnique*, *69*(6), 501–513. https://doi.org/10.1680/jgeot.17.P.124

Pineda, J. A., Suwal, L. P., Kelly, R. B., Bates, L., & Sloan, S. W. (2016). Characterisation of Ballina clay. *Geotechnique*, *66*(7), 556–577. https://doi.org/10.1680/jgeot.15.P.181

Powrie, W., Yang, L. A., & Clayton, C. R. I. (2007). Stress changes in the ground below ballasted railway track during train passage. *Proceedings of the Institution of Mechanical Engineers, Part F: Journal of Rail and Rapid Transit*, *221*(2), 247–261. https://doi.org/10.1243/0954409JRRT95

Sakai, A., Samang, L., & Miura, N. (2003). Partially-drained cyclic behavior and its application to the settlement of a low embankment road on silty-clay. *Soils and Foundations*, *43*(1), 33–46. https://www.jstage.jst.go.jp/article/bpb1993/17/11/17_11_1460/_pdf/-char/ja

Terzaghi, K. (1943). Theory of Consolidation. In *Theoretical Soil Mechanics* (pp. 265–296). https://doi.org/https://doi.org/10.1002/9780470172766.ch13

Tong, J., Wu, T., Guo, L., Yuan, Z., & Jin, H. (2022). Long-term cyclic behavior of soft clay under different variable confining pressures and partially drained conditions. *Transportation Geotechnics*, *33*, 100723. https://doi.org/10.1016/J.TRGEO.2022.100723

Toufigh, M. M., & Ouria, A. (2009). Consolidation of inelastic clays under rectangular cyclic loading. *Soil Dynamics and Earthquake Engineering*, *29*, 356–363. https://doi.org/10.1016/j.soildyn.2008.03.006

Yasuhara, K., Yamanouchi, T., & Hirao, K. (1982). Cyclic Strength and Deformation of Normally Consolidated Clay. *Soils and Foundations*, *22*(3), 77–91. https://doi.org/10.3208/sandf1972.22.3_77

Yıldırım, H., & Erşan, H. (2007). Settlements under consecutive series of cyclic loading. *Soil Dynamics and Earthquake Engineering*, *27*(6), 577–585. https://doi.org/10.1016/j.soildyn.2006.10.007

Zhou, J., & Gong, X. (2001). Strain degradation of saturated clay under cyclic loading. *Canadian Geotechnical Journal*, *38*(1), 208–212. https://doi.org/10.1139/t00-062

Table 1: Summary of past studies related to consolidation under cyclic loading

Sources	Soil types	Stress conditions & sample sizes (Diameter x Height mm)	Characteristics of cyclic load	Frequencies	Total Cyclic loading duration	Drainage condition during cyclic loading	Details
Brown et al., (1977)	Remoulded Norwegian Drammen clay (LL = 55%; PL = 28%)	Triaxial (75x150)	Two-way Sinusoidal wave-form	0.1 Hz	11.1 hours	Not allowed	Undrained cyclic loading tests were performed for 2.7 hrs (1000 cycles) and followed by an overnight drainage period

Fujiwara et al. (1985)	Remoulded Kudamatsu Clay (LL = 65%; PL = 30%)	Oedometer (60x20)	Rectangular step loading	0.023 – 0.004 Hz	96 hours	Allowed	Step loadings were applied along with a sustained static loading
O'reilly et al. (1991)	Remoulded Keuper Marl (mudstone) (LL = 32%; PL = 17%)	Triaxial (76x150)	Two-way Sinusoidal wave-form	0.1 Hz	30 hours	Not allowed	Six hours of undrained cyclic loading followed by 18 hours of rest period
Sakai et al. (2003)	Undisturbed Silty-clay from Saga, Japan (LL = 63%; PL = 31%)	Triaxial (50x100)	One-way Sinusoidal wave-form	0.1 – 1 Hz	250 s	Allowed	Drainage was allowed in the lateral direction using filter papers.

Yildirim & Erşan (2007)	Remoulded clay from Zeytinburnu, Istanbul (LL = 73%; PL = 25%)	Simple shear (70x30)	Two-way Sinusoidal wave-form	0.1 Hz	2500 s	Not allowed	The undrained cyclic load was applied for 500 seconds and followed by 3600 seconds during rest periods
Lei et al. (2020)	Remoulded Tianjin soft clay (LL = 52.7%; PL = 27.1%)	Triaxial (70x140)	One-way Sinusoidal wave-form	0.5 – 2 Hz	0.6 hours (2250 sec)	Not allowed	Undrained intermittent cyclic loading for 750 s followed by a drained rest period of 24 hours
Nie et al. (2020)	Remoulded clay from China	Triaxial (39.1x80)	One-way Sinusoidal wave-form	2 Hz	1.4 hours (5000 sec)	Not allowed	Undrained cyclic loading for 1000 s followed by a drained rest period of 1000 s
Chai et al. (2021)	Remoulded Ariake clay (LL =	Oedometer (485x618)	Rectangular step loading	0.017 Hz (Period 60 s)	1200 hours	Allowed	EPWP was dissipated radially (through PVDs) during step loading

	124.2%; PL = 58.5%)						
Tong et al. (2022)	Remoulded clay form Wenzhou, China (LL = 64%; PL = 38%)	Triaxial (50x100)	One-way Sinusoidal wave-form	1 Hz	13.8 hours (50,000 cycles)	Allowed	No rest period
(Ni & Geng, 2022)	Remoulded Kaolin (LL = 55%; PL = 27%)	Triaxial (300x600)	One-way Sinusoidal wave-form	1 Hz	12.6 hours	Allowed	Cyclic load was applied for 15000 cycles with radial drainage allowed through PVDs and followed by 48 hrs rest period

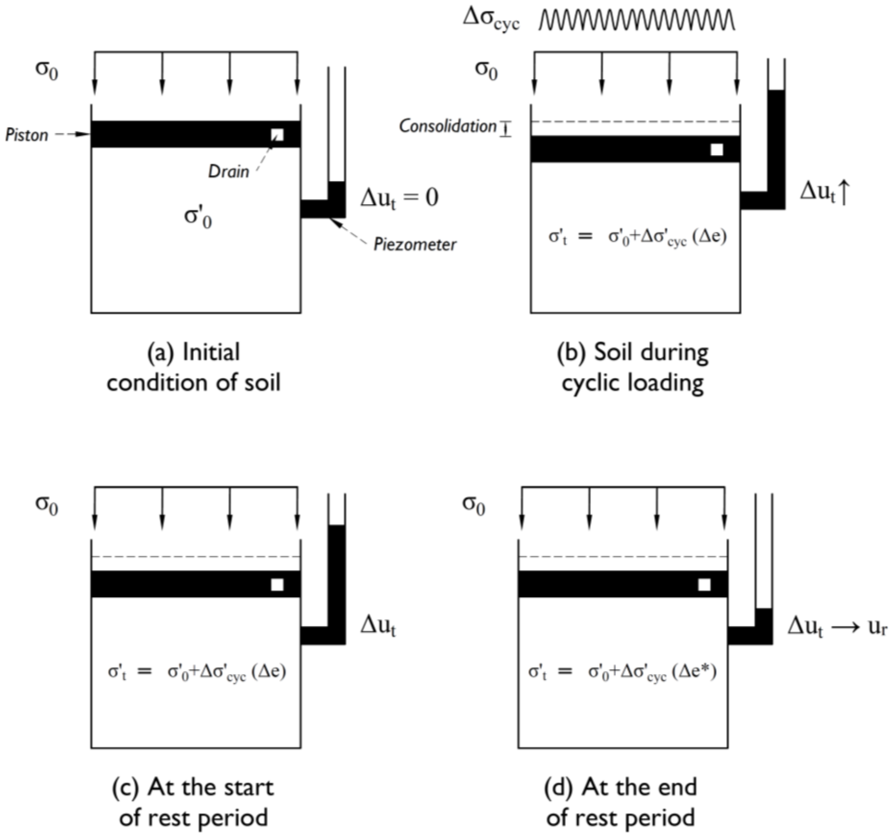

Figure 1: Conceptual piston analogy for consolidation under cyclic loading with rest periods (a) initial condition of soil (b) soil during cyclic loading (c) at the start of rest period (d) at the end of rest period

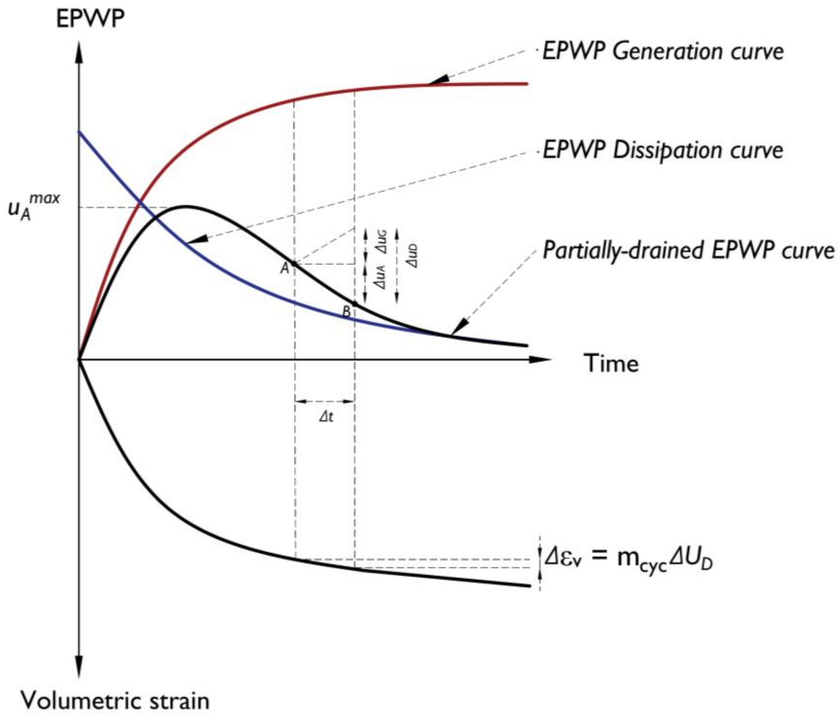

Fig. 2 EPWP and associated volumetric strain under cyclic loading condition (Inspired by Hyodo & Yasuhara (1988))

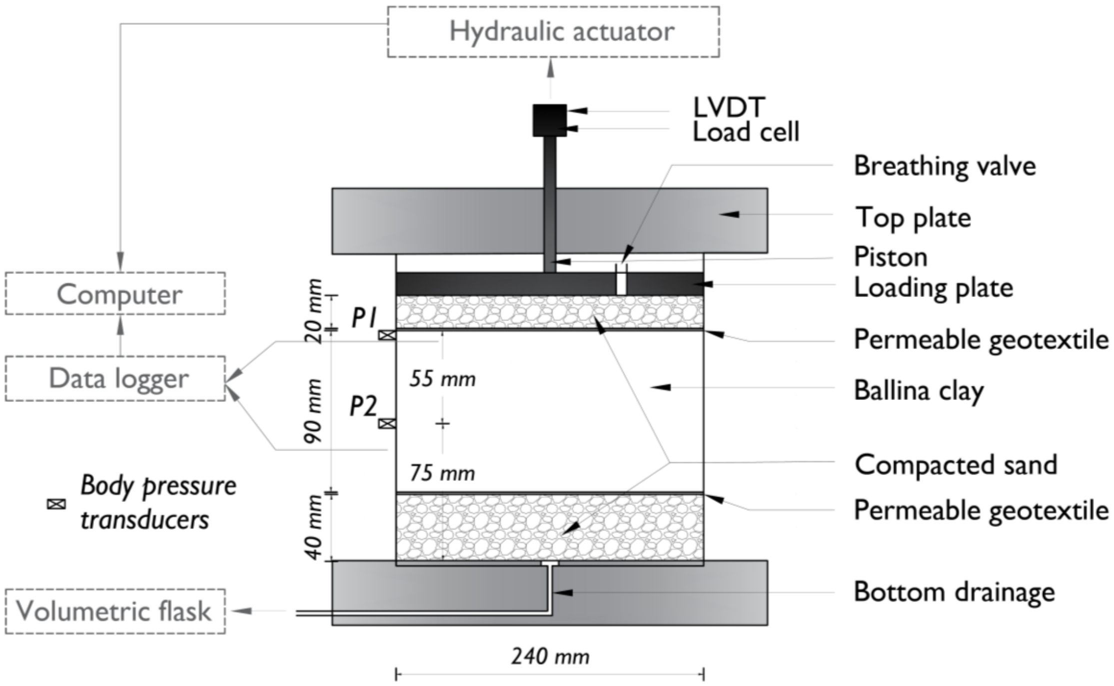

Figure 3: Schematic diagram of the experimental setup

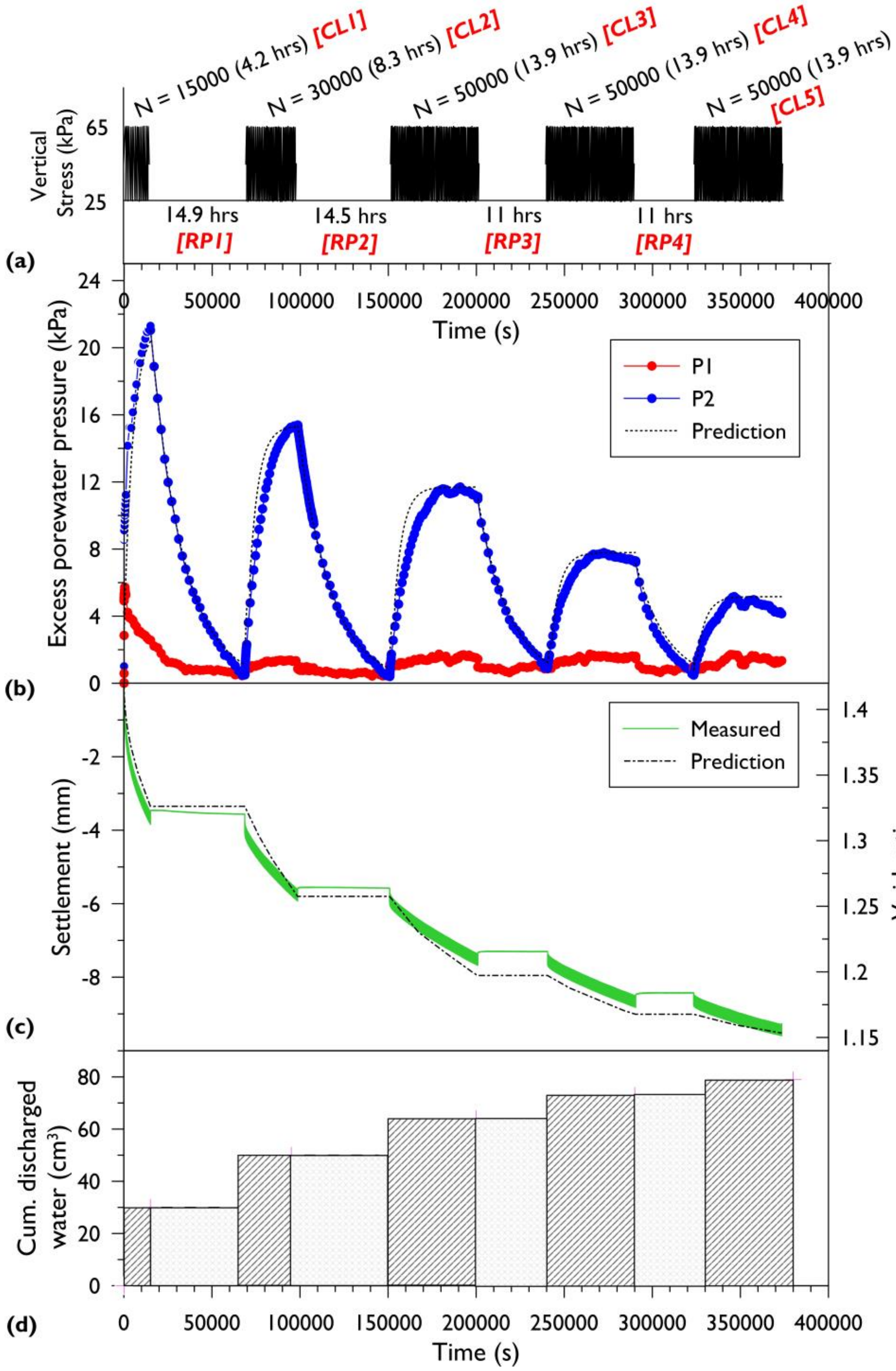

Figure 4: (a) loading schedule; (b) EPWP; (c) settlement; (d) volume of discharged water (CL1, CL2, CL3, CL4, CL5 represent cyclic loading stages 1, 2, 3, 4, 5 respectively; RP1, RP2, RP3, RP4 represent rest periods 1, 2, 3 and 4, respectively)

576

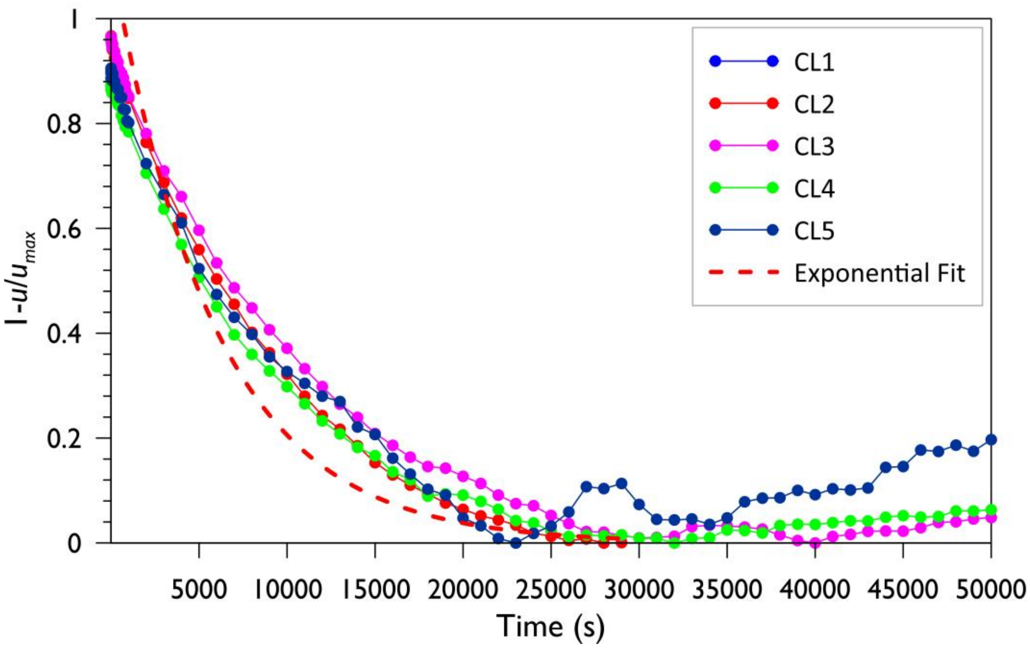

577 Figure 5: Normalised EPWP during cyclic loading

578

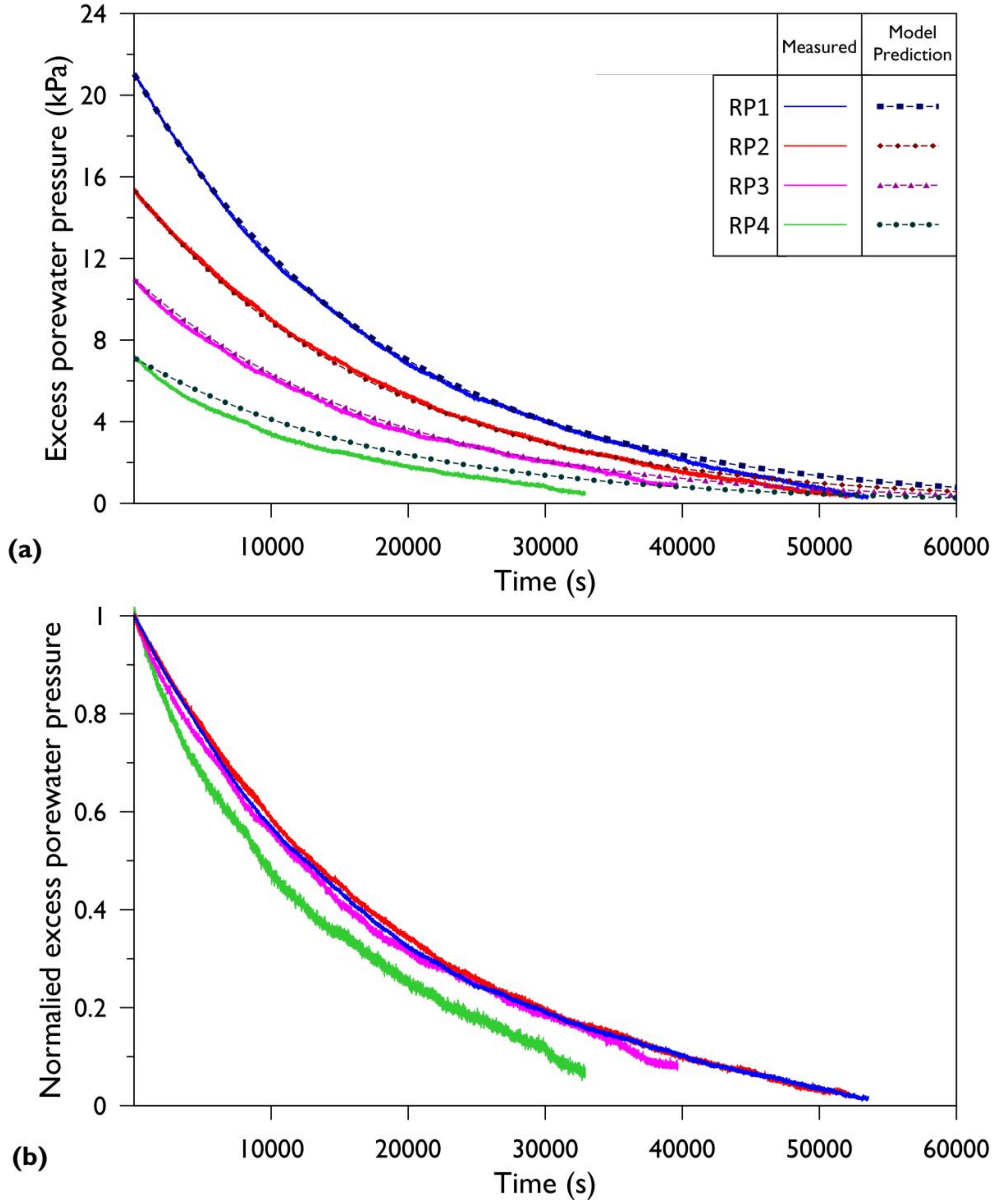

Figure 6: (a) Predicted and measured EPWP at P1 during rest periods (b) normalised EPWP during rest periods

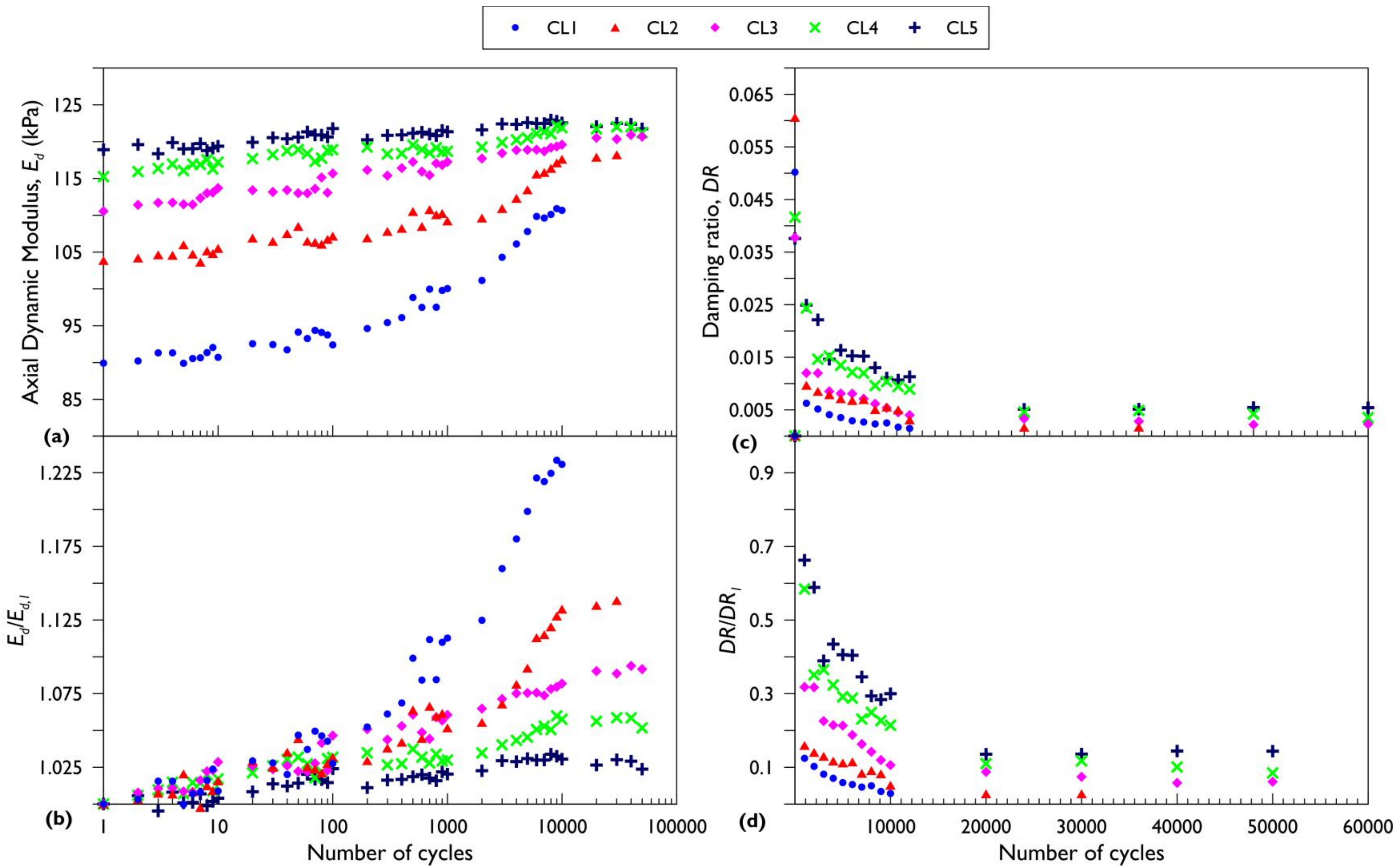

Figure 7: (a) Resilient modulus, (b) normalised resilient modulus, (c) damping ratio and (d) normalised damping ratio

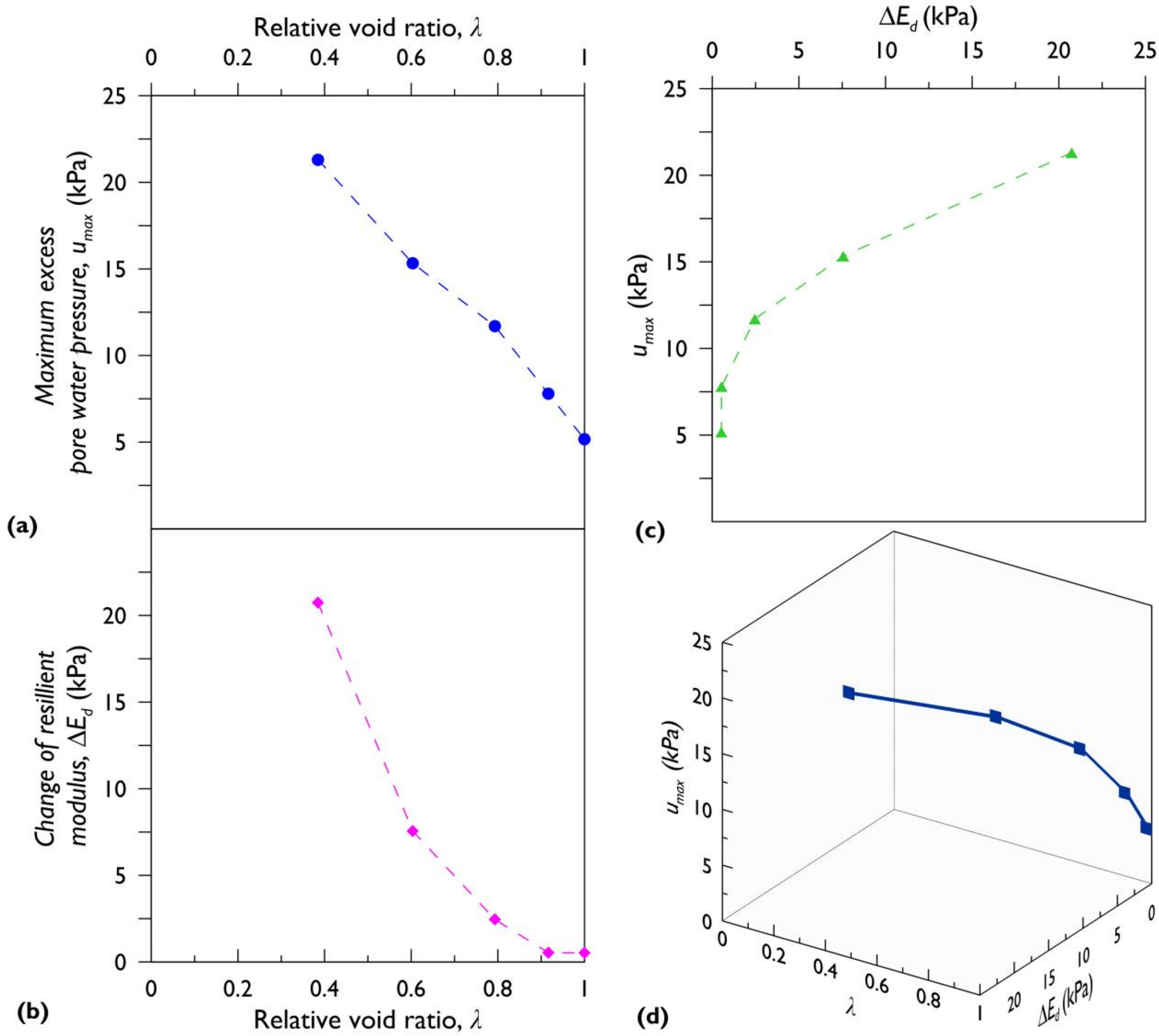

Figure 8: Relationships of (a) maximum EPWP and relative void ratio, (b) change of resilient modulus and relative void ratio, (c) maximum EPWP and change of resilient modulus, and (d) change of resilient modulus, maximum EPWP and relative void ratio in 3D space.

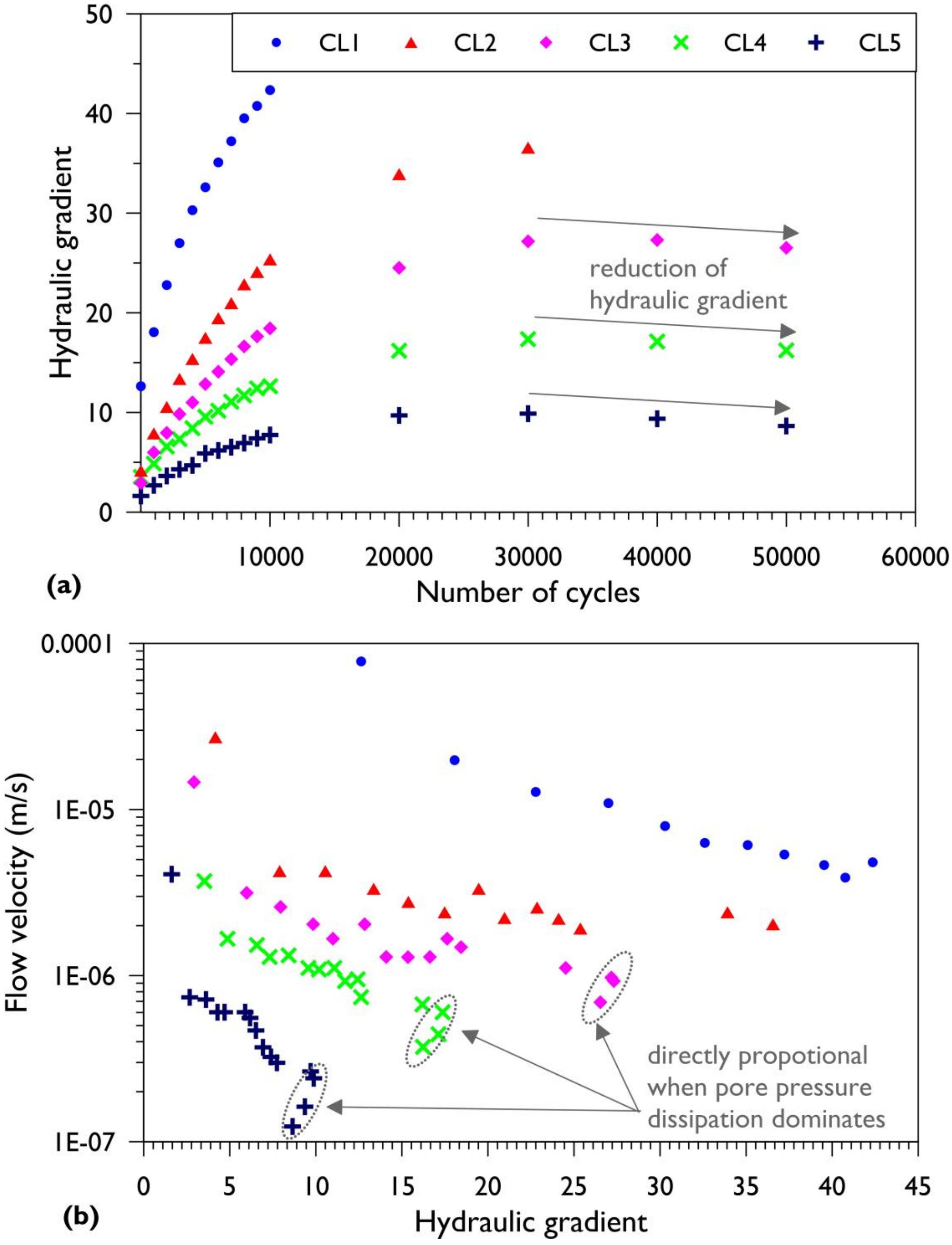

Figure 9: (a) Trend between the hydraulic gradient and the number of cycles; (b) Relationship between the flow velocity and the hydraulic gradient